Frequency Reconfigurable Dual-Band Reflection-Type Phase Shifter with 360° Phase Shift Range for 5G NR FR2 Applications

Munsu Jeong[1], Minji Kang, Kyutaek Oh and Ockgoo Lee[a]
Department of Electrical Engineering, Pusan National University
E-mail : [1]msj3718@pusan.ac.kr

***Abstract* - This paper proposes a frequency reconfigurable dual-band passive 360° reflection-type phase shifter (RTPS) for fifth-generation (5G) applications. The proposed phase shifter provides a full 360° phase shift range in multiple 5G new radio (NR) communication bands—n261 (27.5–28.35 GHz) and n260 (37–40 GHz)—using a transformer-based switchable inductor. The proposed transformer-based switchable inductor allows the operating frequency bands to be changed for achieving maximum phase shift range. Consequently, the proposed RPTS achieves a full 360° phase shift range with average insertion losses of 7.65 ± 2.08 and 7.03 ± 0.15 dB at 28 and 39 GHz, respectively. To the best of our knowledge, the proposed RTPS is the first dual-band RTPS to achieve a 360° phase shift in 5G NR FR2 applications.**

***Keywords*—5G communication, Beamforming, Phased-array system, Reflection-type phase shifter**

I. INTRODUCTION

The release of fifth-generation (5G) new radio (NR) communication systems has garnered significant attention owing to their ability to support high-speed data communication. In millimeter-wave (mm-wave) 5G NR wireless communication systems, multiple frequency range 2 (FR2) frequency bands, such as n260 and n261, are allocated to different countries, as defined by the 3rd Generation Partnership Project (3GPP). Because different 5G NR frequency bands are allocated to each country and region, mm-wave phased-array systems supporting dual-band or broadband are in high demand. To support multiple bands, many researchers have intensified their efforts on power amplifiers [1], low noise amplifiers [2], mixers [3], [4] and phase shifters [5] using band-switchable inductors for optimum resonance at multiple bands. In phased array systems, a phase shifter is a key building block for controlling the phase of each antenna element with a 360° phase shift to perform beamforming. Moreover, for accurate beamforming, the phase shifter in a phased-array system requires low insertion loss, low DC power consumption, a full 360° phase shift range over broad bandwidth, high phase resolution, and high linearity.

An active vector-sum phase shifter (VSPS) can achieve phase shifting with high resolution. However, it suffers from a high noise figure, nonlinearity, and consumes DC power [6]. Conversely, a passive switch-type phase shifter (STPS) is composed of cascaded cells for phase shifting and operates with discrete digital control by switching. An STPS can provide phase shifting with high linearity and zero DC power consumption. However, a drawback of STPS is the trade-off between phase resolution and insertion loss. This typically results in limited phase resolution. By contrast, a passive reflection-type phase shifter (RTPS) can provide a full 360° phase shift with superior linearity, high phase resolution, and zero DC power consumption. Therefore, RTPSs are attractive for high-performance phased-array systems to satisfy the stringent requirements. Among many RTPS topologies, an RTPS terminated with π-type reflective loads is popular [7]–[9]. However, previous works in [7]–[9] show a narrowband operation owing to the fixed inductance of the reflective loads. To support multiple bands with a 360° phase shift range, a frequency reconfigurable STPS using a switchable inductor for dual-band operation was presented [5]. It achieved a low average insertion loss and high return loss; however, it featured a limited phase resolution.

In this work, a frequency reconfigurable dual-band RTPS is proposed to support full 360° phase shift range in the n260 and n261 bands with a transformer-based switchable inductor. To the best of our knowledge, the proposed RTPS is the first dual-band RTPS among reported designs to achieve a 360° phase shift range across multiple 5G NR FR2 frequency bands.

The remainder of this paper is organized as follows: The principle of the RTPS and the proposed frequency reconfigurable dual-band 360° RTPS are explained in Section II. Section III presents the post-layout simulation results of the proposed RTPS. Finally, Section IV summarizes the conclusions of this paper.

a. Corresponding author; olee@pusan.ac.kr

Manuscript Received May 22, 2024, Revised Aug. 19, 2024, Accepted Aug. 19, 2024

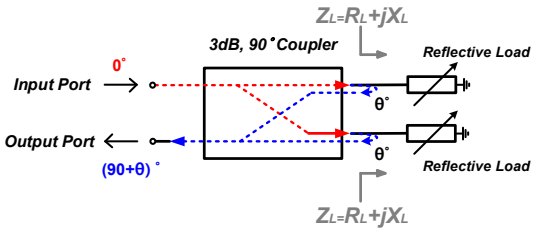

Fig. 1. Operation principle of RTPS.

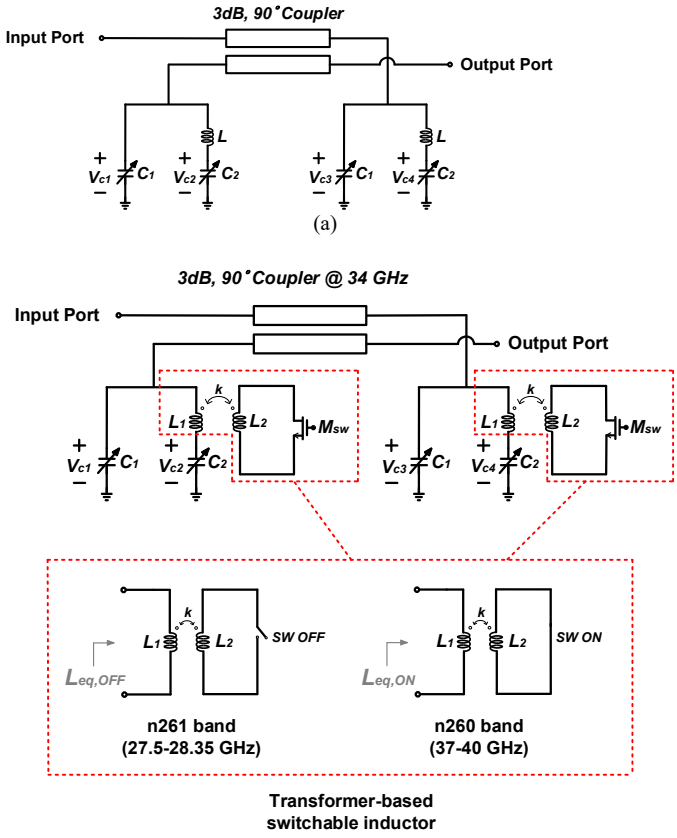

Fig. 2. A 360° RTPS terminated with π-type loads, (a) conventional RTPS, (b) proposed frequency reconfigurable dual-band RTPS.

II. DESIGN OF THE PROPOSED FREQUENCY RECONFIGURABLE DUAL-BAND MMWAVE RTPS

A. Operation principle of proposed RTPS

Fig. 1 shows the conventional RTPS, which consists of a 3-dB quadrature coupler and two identical reflective loads. The input signal is equally divided with a 90° phase difference by a 3-dB quadrature coupler, and the signals are reflected by loads and combined in-phase at the output port. Assuming that the 3-dB quadrature coupler and reflective loads are lossless ($R_L \approx 0$), the phase shift can be derived as:

$$\theta = -90 - 2tan^{-1}\left(\frac{X_L}{Z_O}\right) \quad (1)$$

$$\Delta\theta = 2tan^{-1}\left(\frac{X_{L,max}}{Z_O}\right) - 2tan^{-1}\left(\frac{X_{L,min}}{Z_O}\right) \quad (2)$$

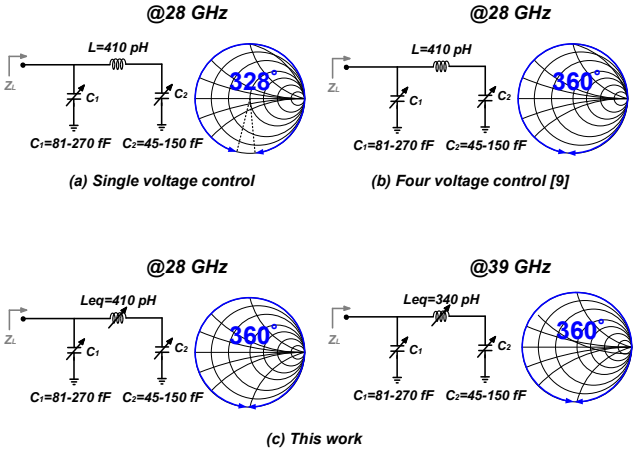

Fig. 3. The load impedance tuning range of π-type networks for (a) single voltage control, (b) four voltage control and (c) proposed structure.

where the phase shift θ, the phase shift range $\Delta\theta$. X_L and Z_O are the reflective load reactance and characteristic impedance of the coupler, respectively. The characteristic impedance of the coupler is commonly set to 50 Ω. From equation (2), the phase shift range of the RTPS is primarily determined by the tuning range of the reflective load impedance. In integrated implementations, the variable capacitance used to adjust impedance tuning can be realized by changing the voltage of a MOS varactor. The tunable reflective load is achieved by a capacitive load or series/parallel L–C tanks for phase shifting. If the reactance X_L can be tuned from $-\infty$ to ∞, it can achieve a full 360° phase shift range. Because the capacitance-tuning range C_{max}/C_{min} of MOS varactors is limited in CMOS technology, these load structures cannot achieve 360° phase shift range [10].

To achieve a large phase shift range, high-order reflective loads are employed in RTPS. Fig. 2(a) shows the conventional RTPS terminated with high-order π-type reflective loads for a large phase shift range. The phase shift θ for the π-type RTPS can be expressed as:

$$\theta = -90 - 2tan^{-1}\left(\frac{1-\omega^2 LC_2}{\omega Z_O(C_1+C_2)\left(\omega^2 L\frac{C_1C_2}{C_1+C_2}-1\right)}\right) \quad (3)$$

The RTPS terminated with π-type loads can achieve up to ~330° phase shift range with proper tuning range C_{max}/C_{min} of 3 by single voltage control ($V_{C1} = V_{C2} = V_{C3} = V_{C4}$) [9]. To achieve a full 360° phase shift range using π-type loads, two stages of RTPS were cascaded with symmetrical reflective loads [7] and a reflective load using a transformer structure was introduced [8]. In [9], asymmetrical π-type loads controlled by four voltages ($V_{C1} \neq V_{C2} \neq V_{C3} \neq V_{C4}$) was proposed to extend the phase shift range from 330° to 360°. However, reflective loads adopting a fixed inductance exhibit narrowband operation, as indicated by equation (3). To support multiple bands, we propose a frequency reconfigurable dual-band RTPS with a transformer-based switchable inductor, as illustrated in Fig. 2(b). The proposed frequency reconfigurable dual-band RTPS can achieve a maximum phase shift range of 330° in the n260 and n261

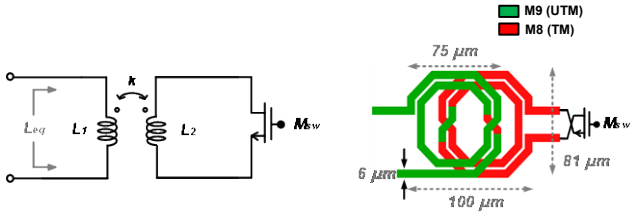

Symbol	Definition	Value
L1 / L2	Primary, secondary winding	364 pH / 419 pH
k	Coupling coefficient	0.41

(a)

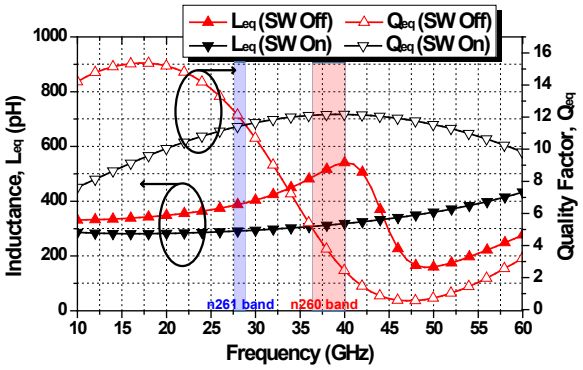

(b)

Fig. 4. (a) Schematic and layout of transformer-based switchable inductor and (b) simulation results.

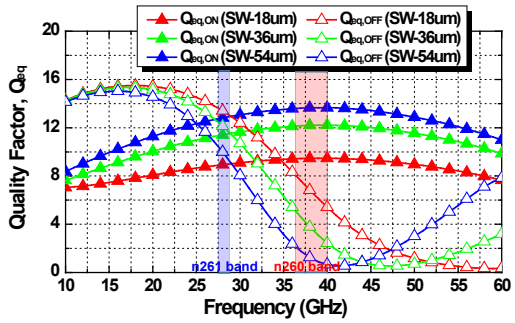

Fig. 5. Simulated equivalent quality factor of transformer-based switchable inductor for different sizes of the NMOS switch.

bands with a switchable inductor using single voltage control. Furthermore, the phase shift range of the proposed RTPS can be extended to 360° by adopting four voltage-controlled asymmetrical loads. In addition, the proposed transformer-based switchable inductor can be applied to the structures reported in [7], [8] to achieve a 360° phase shift range in multiple bands.

B. Proposed structure of RTPS

Fig. 3(a) shows the maximum phase shift range of ~330° with conventional π-type networks by a single voltage control when the inductance is optimized at 28 GHz. The phase shift range can be extended using four voltage controls as shown in Fig. 3(b) [9]. The proposed RTPS can achieve a 330° phase shift range with single voltage using a switchable inductor at 28 and 39 GHz. In addition, the phase shift range

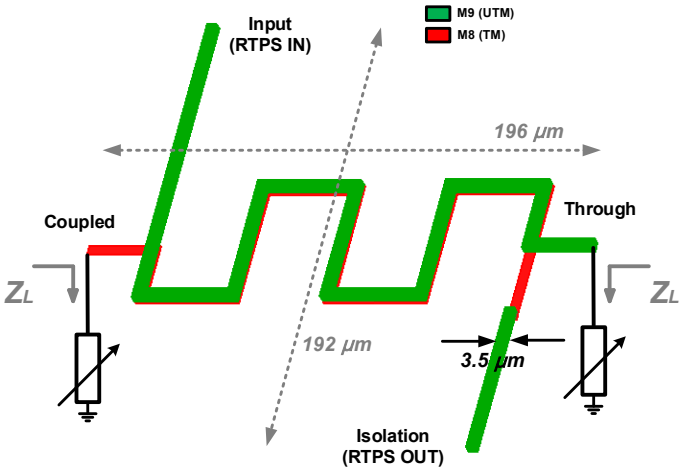

(a)

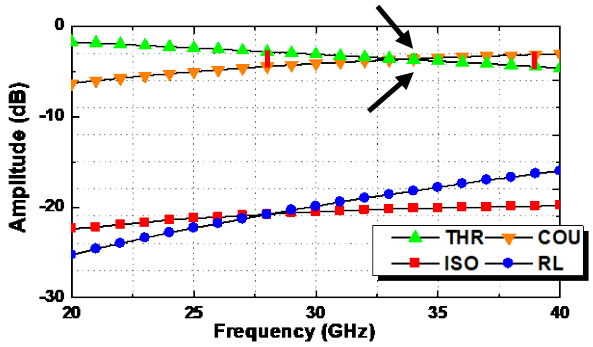

(b)

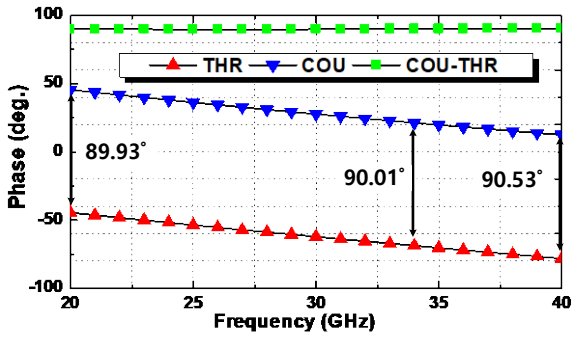

(c)

Fig. 6. (a) Layout of 3-dB quadrature coupler, (b) simulated amplitudes of the through, coupled, isolation ports and the return loss at the input ports and, (c) simulated phase difference between input and output ports.

of the proposed RTPS can be extended from 330 to 360° at 28 and 39 GHz by adopting asymmetrical loads controlled by four voltages as shown in Fig. 3(c). Using equation (3), the required inductances are 410 and 340 pH at 28 and 39 GHz, respectively. To achieve a maximum phase shift range at multiple bands, we introduced a reflective load with a transformer-based switchable inductor.

The proposed frequency reconfigurable dual-band RTPS was designed using 65 nm CMOS technology. The back-end-of-line (BEOL) process of the 65-nm CMOS technology provides 3.4 μm ultra-thick metal (M9) and 0.7 μm thick metal (M8). As shown in Fig. 4(a), the equivalent inductance

L_{eq} with the switch ON/OFF states can be calculated as:

$$L_{eq,ON} \approx L_1(1-k^2) \quad (4)$$

$$L_{eq,OFF} \approx L_1. \quad (5)$$

where k and L_1 are the coupling coefficient and primary inductance of the transformer. From equations (4) and (5), L_{eq} varies depending on the switch ON/OFF states and the calculated k of the transformer was 0.41 for a $L_{eq,ON}/L_{eq,OFF}$ of 340 pH / 410 pH. To achieve calculated k of 0.41, the overlap between the primary and secondary windings is optimized. The metal width of the designed transformer is 6 μm, and the overall transformer size is 100 μm × 81 μm. Fig. 4(b) shows the simulated equivalent inductance and quality factor (Q) of the transformer-based switchable inductor for switching ON/OFF states. An NMOS switch of the transformer-based switchable inductor can be modeled as a resistor or a capacitor according to the ON or OFF states. When the NMOS switch is in the ON state, it is represented by an ON-resistance, and when in the OFF state, it is modeled by an OFF-capacitance [11]. Thus, when the transformer-based switchable inductor is in the ON state of the NMOS switch, the equivalent Q will be degraded due to the presence of the ON-resistance in the secondary winding. As shown in Fig. 4(b), the maximum value of the equivalent Q in the ON state of the NMOS switch is lower than that in the OFF state of NMOS switch. When the transformer-based switchable inductor is in the OFF state of the NMOS switch, the maximum point of the equivalent Q will be shifted to lower frequencies due to the presence of the OFF-capacitance in the secondary winding. Therefore, careful optimization of the switch size is required. Fig. 5 illustrates the simulated equivalent Q of the transformer-based switchable inductor for different sizes of the NMOS switch. As the size of the NMOS switch increases, the OFF-capacitance increases in the OFF state of the NMOS switch, resulting in a decrease in the frequency at which the maximum point of equivalent Q occurs. On the other hand, in the ON state of the NMOS switch, the ON-resistance decreases with increasing the size of the NMOS switch, leading to an improvement in the equivalent Q. Considering these relations, the width of the NMOS switch was chosen for W/L = 36 μm / 0.06 μm. Because the overall circuit performance is typically worse as the operating frequency increases, the size of the NMOS switch, which gives a higher equivalent Q at 39 GHz than that at 28 GHz is selected in this design. An electromagnetic (EM) simulation of the transformer structure was performed, and the EM simulated results are included to characterize the equivalent inductance and quality factor. The simulated equivalent inductances were 410 pH (Q = 11.8) and 337 pH (Q = 12.4) at 28 GHz (V_{sw} = 0 V) and 39 GHz (V_{sw} = 1 V), respectively. This shows that both inductances are close to the required inductances calculated using equation (3) to provide the maximum phase shift range at both frequencies.

A 3-dB quadrature coupler was designed with vertically coupled lines using the M9 and M8 layers, as shown in Fig. 6(a). Because an additional impedance matching can reduce bandwidth performance, the characteristic impedance of the coupler is set to 50 Ω. As shown in Fig. 6(b), the amplitude

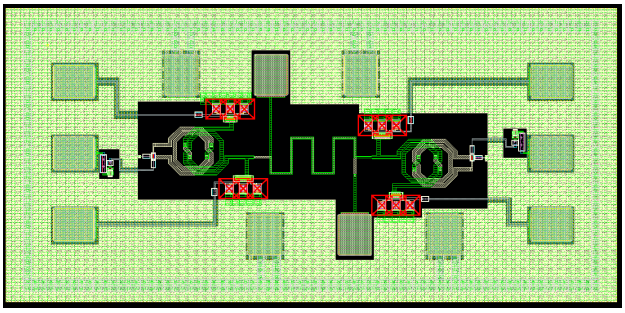

Fig. 7. Layout photograph of the proposed frequency reconfigurable dual-band RTPS.

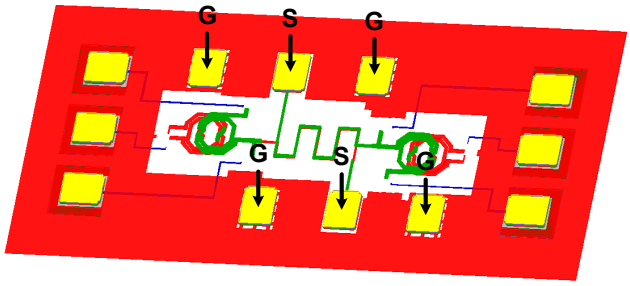

Fig. 8. 3D view of the EM simulated structure.

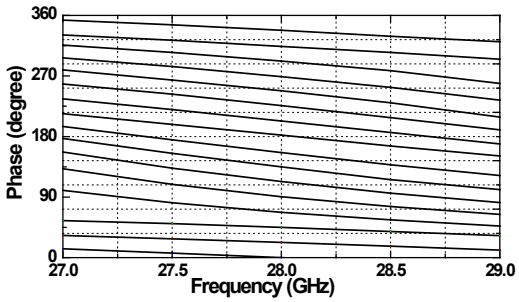

(a)

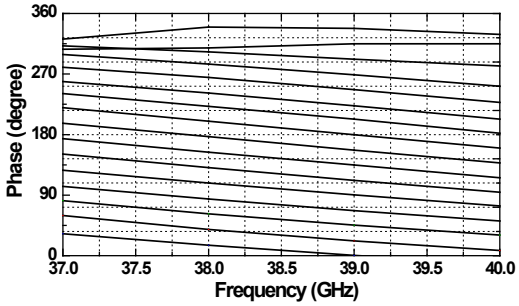

(b)

Fig. 9. Simulated phase shift of 16 states versus frequency when V_{sw} was (a) 0 V and (b) 1 V.

responses of the through and coupled ports are -3.7 and -3.6 dB at 34 GHz, respectively. The coupler introduces 0.7 dB, considering a 3-dB loss from 1:2 power splitting. In addition, the amplitude imbalance of the through and coupled ports is only 1.7 and 1.2 dB at 28 and 39 GHz, respectively. The insertion loss of a reflection-type phase shifter can be increased due to amplitude imbalance of a 3-dB quadrature coupler. In this design, we have mitigated amplitude imbalance at the high frequency band, although this requires some compromise in performance at the lower frequency band.

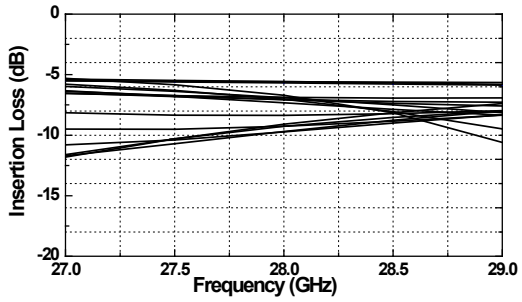

(a)

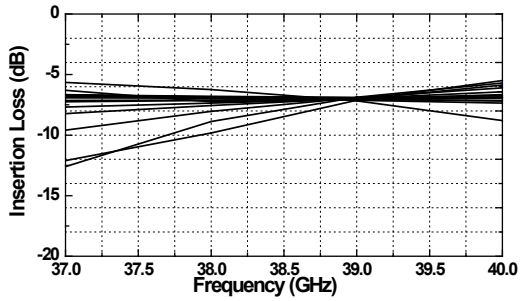

(b)

Fig. 10. Simulated insertion loss of 16 states versus frequency when V_{sw} was (a) 0 V and (b) 1 V.

Fig. 6(c) shows the phase responses of the through and coupled ports. The phase difference between the through and coupled ports maintains approximately 90°, with a phase error of <0.53° across 20–40 GHz. Therefore, the 3-dB quadrature coupler exhibits relatively broadband amplitude and phase responses with a low insertion loss. Accumulation-mode MOS varactors, C_1 and C_2 are designed using the length of 0.27 μm and a finger width of 1.4 μm (C_1: 42 fingers x 1.4 μm and C_2: 24 fingers x 1.4 μm). The capacitance tuning ranges of C_1 and C_2 are designed to ~3.4 ($C_{1,max}/C_{1,min}$ = 280 fF / 80 fF and $C_{2,max}/C_{2,min}$ = 158 fF / 46 fF) and Q~10.

III. POST-LAYOUT SIMULATION RESULTS

The proposed frequency reconfigurable dual-band RTPS was designed using 65-nm CMOS technology. The layout of the designed RTPS is illustrated in Fig. 7. The total core area is approximately 0.18 mm^2 with a 3-dB quadrature coupler and reflective loads. All parasitic capacitors and resistors in the varactors and NMOS switch were extracted and reflected in the total circuit simulation. A post-layout simulation was performed using the ADS Momentum simulator. To include interactions among all routings, pads, and the ground plate, all these elements were included in the EM simulation setup. Fig. 8 shows the 3D view of the EM simulated structure. It is crucial to note that an ideal ground is only considered at the ground pad area where it aligns with the probe tips, and the ground connections within the chip itself are not ideal to consider ground network effect [12]. Fig. 9 depicts the simulated phase shift of 16 states when V_{sw} is 0 and 1 V. All varactor voltage settings were selected to achieve a full

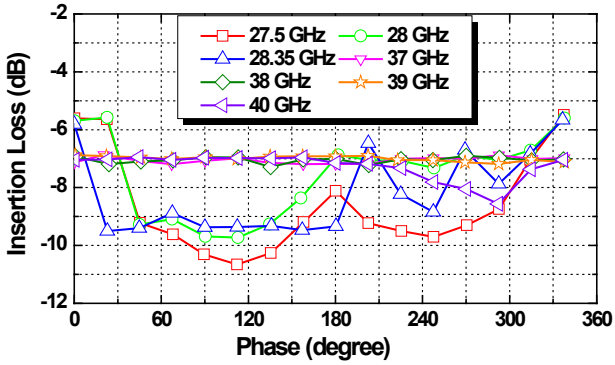

Fig. 11. Simulated insertion losses for different operating frequencies.

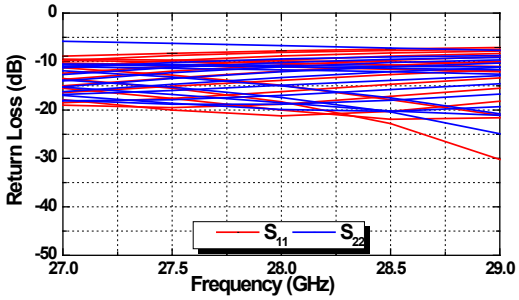

(a)

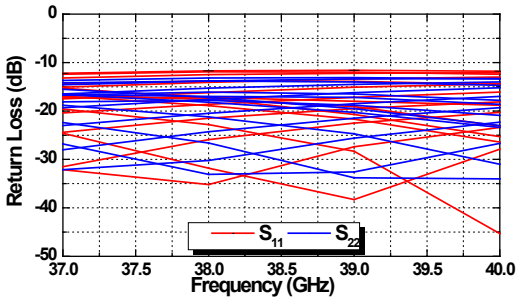

(b)

Fig. 12. Simulated return loss of 16 states versus frequency when V_{sw} was (a) 0 V and (b) 1 V.

360° phase shift range with uniform insertion loss at 28 and 39 GHz. Fig. 9 shows that the phases were nearly distributed throughout the entire 360° at both 27.5–28.35 and 37–40 GHz. As shown in Fig. 10, the insertion losses were 7.65 ± 2.08 and 7.03 ± 0.15 dB for the selected voltage settings at 28 and 39 GHz, respectively. Fig. 11 shows the simulated insertion losses for different operating frequencies in the n260 and n261 bands. All varactor voltage settings were reselected for each operating frequency. It shows that the proposed RTPS can achieve a 360° phase shift range at each operating frequency with low loss variation. Fig. 12 shows that the simulated input and output match for all the voltage settings at 27.5–28.35 and 37–40 GHz. A worst-case return loss of 6.2 dB at 27.5 GHz occurs with asymmetrical voltage control. Table I summarizes the performance of the proposed phase shifter and compares its results with those of mm-wave phase shifters reported in previous works. The results demonstrate that this work achieves zero DC power consumption, low insertion loss, and a full 360° phase shift range with high phase resolution in the two operating bands.

TABLE I. Comparison with Prior-art mm-wave Phase Shifters.

Reference	Process	Type/bits	Frequency [GHz]	Gain [dB]	Return Loss [dB]	Core Area [mm^2]
[13] RFIC2018	65nm CMOS	RTPS/360°	29	-8.3±0.2	23	0.076
[9] TMTT2017	65nm CMOS	RTPS/360°	28	-7.75±0.3	6.7	0.16
[14] TCAS-I2023	130nm SiGe BiCMOS	VSPS/6bits	18–30	1.75±2.75 @22GHz	5**	0.28
[15] MWCL2020	65nm CMOS	STPS/5bits	27–42	-12±1.4 @37GHz	7	0.33
[16] MWCL2020	28nm CMOS	STPS/4bits	29–37	-12.8±2.5 @33GHz	10	0.08
[5] TCAS-II2021	65nm CMOS	STPS/5bits	26.5–29.5	-7.9±1 @28GHz	13.2	0.26
			37–40	-9.3±1 @39GHz	10.4	
*This Work	65nm CMOS	RTPS/360°	27.5–28.35	-8.08±2.59 @27.5GHz -7.65±2.08 @28GHz -7.58±1.92 @28.35GHz	6.2	0.18
			37–40	-7.03±0.16 @37GHz -7.1±0.2 @38GHz -7.03±0.15 @39GHz -7.76±0.81 @40GHz	11.6	

*Simulated results
**Graphically estimated.

IV. CONCLUSION

This paper proposes a frequency reconfigurable dual-band RTPS with a transformer-based switchable inductor. The structure was developed in a compact 0.18 mm^2 core area using 65 nm CMOS technology. The proposed phase shifter achieves a full 360° phase shift range with low insertion losses at 28 and 39 GHz, which are part of the 5G NR FR2 frequency bands. This design has low insertion losses of 7.65 ± 2.08 and 7.03 ± 0.15 dB at 28 and 39 GHz, respectively. The return losses remain below -6.2 dB for all voltage settings at 27.5–28.35 and 37–40 GHz. Compared with previously reported fully integrated RTPSs in silicon, these results show that the proposed structure achieves the first-ever full 360° phase shift range at multiple bands among reported RTPS with 360° phase shifting.

ACKNOWLEDGMENT

This work was supported by a 2-Year Research Grant of Pusan National University.

The chip fabrication and EDA tool were supported by the IC Design Education Center (IDEC), Korea.

REFERENCES

[1] J. Lee, J.-S. Paek, and S. Hong, “Millimeter-wave frequency reconfigurable dual-band CMOS power amplifier for 5G communication radios,” IEEE Transactions on Microwave Theory and Techniques, vol. 70, no. 1, pp. 801–812, Jan. 2022.

[2] B. Bae, E. Kim, S. Kim, and J. Han, “Dual-band CMOS low-noise amplifier employing transformer-based band-switchable load for 5G NR FR2 applications,” *IEEE Microwave and Wireless Technology Letters*, vol. 33, no. 3, pp. 319– 322, Mar. 2023.

[3] E. Kim, S. Kim, G. Kim, and J. Han, “Dual-band CMOS down-conversion mixer adopting band-switchable transformer,” *IEEE Transactions on Circuits and Systems II: Express Briefs*, vol. 70, no. 10, pp. 3902–3906, Oct. 2023.

[4] B. Bae, J. Jeong, S. Kim, J. Lee, K. Kwon, and J. Han, “24–40 GHz dual-band highly linear CMOS up- conversion mixer for mmWave 5G NR FR2 cellular applications,” *IEEE Microwave and Wireless Components Letters,* vol. 32, no. 8, pp. 999–1002, Aug. 2022.

[5] Y.-H. Lin and Z.-M. Tsai, “Frequency-reconfigurable phase shifter based on a 65-nm CMOS process for 5G applications,” *IEEE Transactions on Circuits and Systems II: Express Briefs*, vol. 68, no. 8, pp. 2825–2829, Aug. 2021.

[6] D. Pepe and D. Zito, “Two mm-wave vector modulator active phase shifters with novel IQ generator in 28 nm FDSOI CMOS,” *IEEE Journal of Solid-State Circuits*, vol. 52, no. 2, pp. 344–356, Feb. 2017.

[7] J.-C. Wu, C.-C. Chang, S.-F. Chang, and T.-Y. Chin, “A 24-GHz full-360◦ CMOS reflection-type phase shifter MMIC with low loss-variation,” in Proc. *IEEE Radio Frequency Integrated Circuits Symposium (RFIC)*, Atlanta, GA, USA, 2008, pp. 365–368

[8] A. Basaligheh, P. Saffari, S. Rasti Boroujeni, I. Filanovsky, and K. Moez, “A 28–30 GHz CMOS reflection-type phase shifter with full 360◦ phase shift range,” *IEEE Transactions on Circuits and Systems II: Express Briefs*, vol. 67, no. 11, pp. 2452–2456, Nov. 2020.

[9] A. R. Garg and A. S. Natarajan, “A 28-GHz low-power phased-array receiver front-end with 360◦ RTPS phase shift range,” *IEEE Transactions on Microwave Theory and Techniques*, vol. 65, no. 11, pp. 4703–4714, Nov. 2017.
[10] T.-W. Li and H. Wang, “A millimeter-wave fully integrated passive reflection-type phase shifter with transformer-based multi-resonance loads for 360◦ phase shifting,” IEEE *Transactions on Circuits Systems I: Regular Papers*, vol. 65, no. 4, pp. 1406–1419, Apr. 2018.
[11] B. Razavi, Design of Analog CMOS Integrated Circuits, 2nd ed., McGraw-Hill, pp. 15-30, 2016.
[12] M. H. Montaseri, J. P. Aikio, T. Rahkonen, and A. Pärssinen, “Analysis and design of capacitive voltage distribution stacked MOS millimeter wave power amplifiers,” IEEE Trans. Circuits Syst. I, Reg. Papers, vol. 69, no. 9, pp. 3540–3553, Sep. 2022.
[13] P. Gu and D. Zhao, “Ka-band CMOS 360◦ reflective type phase shifter with ±0.2 dB Insertion loss variation using triple-resonating load and dual-voltage control techniques,” in Proc. *IEEE Radio Frequency Integrated Circuits Symposium (RFIC)*, pp. 140–143, Jun. 2018.
[14] Yu et al., “An 18~30 GHz vector-sum phase shifter with two-stage transformer-based hybrid in 130-nm SiGe BiCMOS,” IEEE *Transactions on Circuits Systems I: Regular Papers*, vol. 70, no. 12, pp. 1–14, Aug. 2023.
[15] J.-H. Tsai, Y.-L. Tung, and Y.-H. Lin, “A 27–42-GHz low phase error 5-bit passive phase shifter in 65-nm CMOS technology,” *IEEE Microwave and Wireless Components Letters*, vol. 30, no. 9, pp. 900–903, Sep. 2020.
[16] M. Jung and B.-W. Min, “A compact Ka-band 4-bit phase shifter with low group delay deviation, *IEEE Microwave and Wireless Components Letters*, vol. 30, no. 4, pp. 414–416, Apr. 2020.

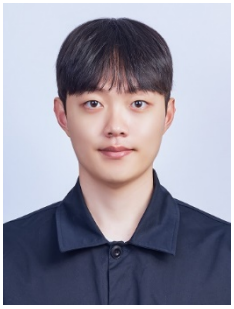

Munsu Jeong received the B.S. degree in Electrical Engineering from Pusan National University, Busan, Korea, in 2024, and is currently pursuing the M.S. degree in electrical engineering at Pusan National University, Busan, Korea. His research interests include RF/mm-wave integrated circuits for mobile applications.

Minji Kang is currently pursuing a B.S in Electrical Engineering from Pusan National University, Busan, Korea. Her research interests include RF/mm-wave integrated circuits for mobile applications.

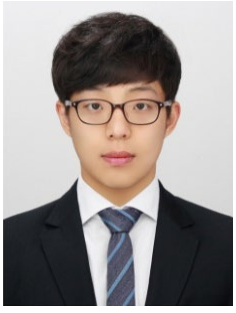

Kyutaek Oh received the B.S. and M.S. degrees in Electrical Engineering from Pusan National University, Busan, Korea, in 2017 and 2022, respectively, and is currently working toward a Ph.D. degree in Electrical Engineering at Pusan National University, Busan, Korea.
His research interests include mm-wave power amplifier design for mobile applications and DC-DC converters.

Ockgoo Lee received the B.S. degree in electrical engineering from Sungkyunkwan University, Korea, in 2001, the M.S. degree in electrical engineering from the KAIST, Korea, in 2005, and the Ph.D. degree in electrical and computer engineering from the Georgia Institute of Technology, USA, in 2009.
Upon completion of the doctoral degree, he joined Qualcomm Inc., USA, as a Senior Engineer, where he was involved in the development of transmitters and integrated passive circuits on mobile applications. He is currently a faculty member with the Department of Electrical Engineering, Pusan National University, Korea. His research interests include high-frequency integrated circuits and system design for wireless communications.